Pergamon

International Journal of Machine Tools & Manufacture 42 (2002) 1181–1193

INTERNATIONAL JOURNAL OF
MACHINE TOOLS
& MANUFACTURE
DESIGN, RESEARCH AND APPLICATION

Mathematical model of multiflute drill point

Jung-Fa Hsieh, Psang Dain Lin *

National Cheng Kung University, Department of Mechanical Engineering, Tainan, Taiwan 70101

Received 12 November 2001; received in revised form 8 April 2002; accepted 10 April 2002

Abstract

Multiflute drilling is an efficient means of making high accuracy holes without reaming. Because of the current lack of a comprehensive mathematical model for this kind of drilling, this paper presents a complete and simple method for designing multiflute drills. There are three special features of the proposed model. The first is that rotational axial-type cutting tools and disk-type abrasive wheels are modeled by revolution geometry, so that the normals and tangent vectors of flute and flank surfaces can be obtained explicitly. Consequently, rake and clearance angles of cutting and chisel edges can be investigated according to recommended ISO standards. The second feature is that the mathematical models of flute and flank surfaces are integrated, so that cutting and chisel edges and their various characteristic angles can be obtained by numerical calculation. Finally, a simple way to determine the rake angles and wedge angles and clearance angles is presented by using the unit normals of the ISO-recommended reference planes. To verify the validity of this methodology, a designed three-fluted drill was machined on a 6-axis tool-grinding machine. This model is comprehensive, simple, easy to use, and capable of describing a wide range of drill design features. © 2002 Published by Elsevier Science Ltd.

Keywords: Rake angle; Wedge angle; International standard (ISO); Multiflute drill

1. Introduction

Drills are among the most common metal-working tools. Nevertheless, they present one of the most complex and least understood mechanisms of chip-removal. Thus the design of drill flanks and flutes must be studied, and better modeling tools must be provided, in order to improve drill performance.

Helical flutes are usually machined from cylindrical stock by grinding with disk-type abrasive wheels or milling with axial-type cutting tools. Due to the non-rectilinear motion of the tool along the helical cutting path, the geometry of the machined surface generated on the workpiece is not related simply to the cross-sectional profile of the cutting tool [1]. Recently, three different approaches have been developed for relating the tool profile to the helical profile. One of these methods considers the tool as being composed of infinitely thin disks stacked side by side, the disks being of different diameters that correspond to the tool profile. The helical flute shape is developed as the envelope of the superposed cutting paths of these disks. The second method is based upon calculating the contact 3D space curve of the final grinding operation [2]. The tool profile and the helical groove profile are each mathematically related to the contact curve. Kang et al. [3] developed a third model by utilizing the principles of differential geometry and kinematics to study the inverse and direct problems of helical flute machining.

Another important geometry that affects the drill point is the flank surfaces. Small variations in flank geometry can have a very strong influence on drill performance. The available drill point geometries in the literature are planar [4], conical [5], spiral [6], cylindrical [7], multifacet [8], split [9], and helical micro-drill [10]. For the conventional twist drill, Galloway [5] developed a conical grinding principle. Fujii et al. [11,12] assumed that the flute contour could be described in terms of parameteric equations and utilized computers to analyze drill geometry. Fujii [13] also investigated the effects of chisel edges on conical drill performance to obtain optimum design. In 1979, Tsai and Wu [14] developed a quadratic flank model, including conical, hyperboloidal, and elipsoidal flanks, with applicability to the process of grind-

* Corresponding author. Fax: +886-6-2080-563.
E-mail address: pdlin@mail.ncku.edu.tw (P.D. Lin).

0890-6955/02/$ - see front matter © 2002 Published by Elsevier Science Ltd.
PII: S0890-6955(02)00044-5

Nomenclature

$(xyz)_\circ$ Coordinate frame $(xyz)_\circ$ built in drill;
$(xyz)_t$ Coordinate frame $(xyz)_t$ built in grinding wheel;
${}^\circ A_{t,i}$ The configuration matrix of frame $(xyz)_t$ with respect to drill frame $(xyz)_\circ$ when the grinding wheel generates the ith flute surface;
${}^\circ \Lambda_{t,i}$ The configuration matrix of frame $(xyz)_t$ with respect to drill frame $(xyz)_\circ$ when a form grinding wheel generates the ith flank surface;
${}^t q = [x(h)\ 0\ z(h)\ 1]^T$ The generating curve of a revolution surface;
${}^t r = \mathrm{Rot}(z,v){}^t q$ The revolution surface;
${}^t t = \mathrm{Rot}(z,v){}^t \varepsilon$ The unit tangent vector of the grinding wheel;
${}^t n = [n_x\ n_y\ n_z\ 0]^T$ The unit normal vector of the of the grinding wheel;
$r_{\mathrm{flute},i} = [r_{ix}\ r_{iy}\ r_{iz}\ 1]^T$ The ith drill flute surface;
$n_{\mathrm{flute},i} = [n_{ix}\ n_{iy}\ n_{iz}\ 0]^T$ The unit outward normal of the ith drill flute surface;
$t_{\mathrm{flute},i} = [t_{ix}\ t_{iy}\ t_{iz}\ 0]^T$ The unit tangent vector of the ith drill flute surface;
$R_{\mathrm{flank},i} = [R_{ix}\ R_{iy}\ R_{iz}\ 1]^T$ The ith drill flank surface;
$N_{\mathrm{flank},i} = [N_{ix}\ N_{iy}\ N_{iz}\ 0]^T$ The unit outward normal of the ith drill flank surface;
$T_{\mathrm{flank},i} = [T_{ix}\ T_{iy}\ T_{iz}\ 0]^T$ The unit tangent vector of the ith drill flank surface;
$\underline{\mathbf{R}}_{\mathrm{edge},i} = [\underline{\mathbf{R}}_{ix}\ \underline{\mathbf{R}}_{iy}\ \underline{\mathbf{R}}_{iz}\ 1]^T$ The ith cutting edge;
$\underline{\mathbf{n}}_{\mathrm{edge\ at\ flute},i} = [\underline{\mathbf{n}}_{ix}\ \underline{\mathbf{n}}_{iy}\ \underline{\mathbf{n}}_{iz}\ 0]^T$ The unit normal of flute along the ith cutting edge;
$\underline{\mathbf{N}}_{\mathrm{edge\ at\ flank},i} = [\underline{\mathbf{N}}_{ix}\ \underline{\mathbf{N}}_{iy}\ \underline{\mathbf{N}}_{iz}\ 0]^T$ The unit normal of flank along the ith cutting edge;
$\underline{\mathbf{T}}_{\mathrm{edge},i} = [\underline{\mathbf{T}}_{ix}\ \underline{\mathbf{T}}_{iy}\ \underline{\mathbf{T}}_{iz}\ 0]^T$ The unit tangent vector of along the ith cutting edge;
$\underline{\underline{R}}_{chisel,i} = [\underline{\underline{R}}_{ix}\ \underline{\underline{R}}_{iy}\ \underline{\underline{R}}_{iz}\ 1]^T$ The ith chisel edge;
$\underline{\underline{N}}_{\mathrm{chisel\ on\ flank},i}$ The unit normal on the ith flank surface and along the chisel edge;
$\underline{\underline{T}}_{\mathrm{chisel},i} = [\underline{\underline{N}}_{ix}\ \underline{\underline{N}}_{iy}\ \underline{\underline{N}}_{iz}\ 0]^T$ The unit tangent vector along the ith chisel edge; $\underline{\mathscr{L}}_a$ The unit normal of plane $\underline{\mathbf{P}}_a$.

ing. There have also been investigations of drill wandering motion [15] and drill geometry measurement [16].

From the above, it can be found that only two-fluted drills have been modeled in the literature. However, recent work by Ema et al. [17,18] and Agapiou [19,20] has shown that multiflute drilling is an efficient means of making holes with high accuracy and no reaming. Moreover, the whirling vibrations which frequently occur in ordinary two-fluted drills disappear when a three-fluted drill is used, thereby eliminating rifling marks on the hole surface [17,18]. Consequently, holes with high roundness and straightness are obtained by three-fluted drills. However, a comprehensive mathematical model for multiflute drills is missing. Therefore, this paper introduces a step-by-step generalized mathematical model of a multiflute drill. Section 2 studies axial-type cutting tools and disk-type abrasive tools in terms of revolution geometry, and then establishes their unit normals and tangent vectors. In Section 3, is determined by conjugate surface theory the flute surfaces of a drill with n flutes. Then, in Section 4, the design of flanks is introduced by a general flank model having $z = f(x)$ as its generating curve. Sections 5 and 6 present the determination of cutting and chisel edges and their various cutting angles. To investigate drill performance, numerical calculations of rake, wedge and clearance angles, according to ISO standards, are presented in Section 7. Conclusions are presented in Section 8.

In this paper, a position vector $a_x i + a_y j + a_z k$ is written as a column matrix $j_a = [a_x, a_y, a_z, 1]^T$. Here the pre-superscript 'j' of the leading symbol j_a means this vector is referred with respect to coordinate frame $(xyz)_j$. Given a point j_a, its transformation ${}^k a$ is represented by the matrix product ${}^k a = {}^k A_j\, {}^j a$, where ${}^k A_j$ is a 4×4 matrix defining the position and orientation (referred to as configuration hereafter) of a frame $(xyz)_j$ with respect to another frame $(xyz)_k$ [21]. These notation rules are also applicable to a unit directional vector $j_n = [n_x, n_y, n_z, 0]^T$. If a vector is referred to the drill frame $(xyz)_o$, then its pre-superscript '0' will be omitted for reasons of simplicity.

2. Grinding tool model from surfaces of revolution

In this paper, the term tool (or tools) will be taken to mean high rotational axial-type cutting tools or disk-type abrasive wheels. One important feature of these tools is that their working surfaces are surfaces of revolution. Consequently, these working surfaces are studied in terms of revolution geometry, and their unit normals and tangent vectors are established. A tool surface ${}^t r$ can be obtained by rotating its generating curve ${}^t q = [\mathrm{x}(h)\ 0\ z(h)\ 1]^T$ ($x(h) > 0$ and parameter h varies over a specified range) in xz plane about its symmetrical rotating z_t axis (see Fig. 1). That is

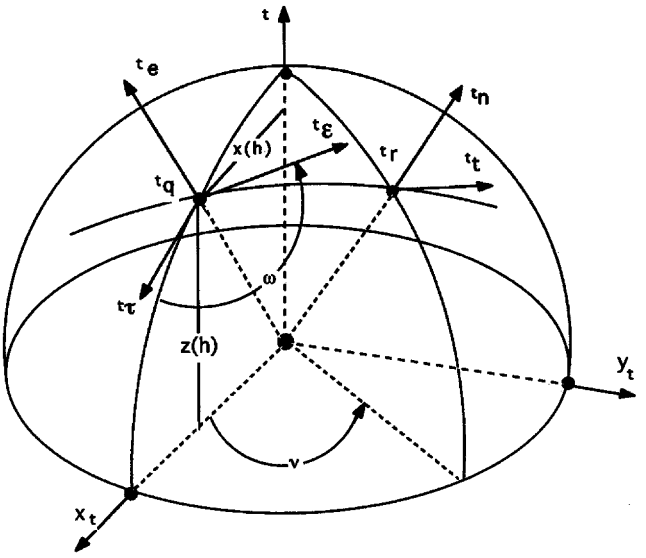

Fig. 1. The generating curve and its unit outward normal and unit tangent vector.

$$ {}^{t}r = \mathrm{Rot}(z,v)\,{}^{t}q = [x(h)\mathrm{C}v\ x(h)\mathrm{S}v\ z(h)\ 1]^{\mathrm{T}} \tag{1} $$

where $\mathrm{Rot}(z,v)$ is the rotation transformation matrix about the z-axis given by (A1) in the Appendix. C and S denote COSINE and SINE, respectively. Eq. (1) is a generalized expression valid for parametrizing the working surfaces of disk and axial-type tools in terms of h and the polar angular position v.

The derivative of a position vector ${}^{t}q$ to this space curve, with respect to arc length s along the curve, is a unit tangent vector to the curve pointing in the direction of increasing arc length. We denote this unit tangent vector by t_τ,

$$ {}^{t}\tau = [\tau_x\ \tau_y\ \tau_z\ 0]^{\mathrm{T}} = \frac{\mathrm{d}({}^{t}q)}{\mathrm{d}s} = \left[\frac{\mathrm{d}x}{\mathrm{d}s}\ 0\ \frac{\mathrm{d}z}{\mathrm{d}s}\ 0\right]^{\mathrm{T}} $$

$$ = \left[\frac{\mathrm{d}x}{\mathrm{d}h}\frac{\mathrm{d}h}{\mathrm{d}s}\ 0\ \frac{\mathrm{d}z}{\mathrm{d}h}\frac{\mathrm{d}h}{\mathrm{d}s}\ 0\right]^{\mathrm{T}} \tag{2} $$

$$ = \left[\frac{x'(h)}{\sqrt{x'(h)^2 + z'(h)^2}}\ 0\ \frac{z'(h)}{\sqrt{x'(h)^2 + z'(h)^2}}\ 0\right]^{\mathrm{T}} $$

Hereafter a prime is used to denote differentiation with respect to the parameter h. Since t_τ is a unit vector, the derivative $\mathrm{d}({}^{t}\tau)/\mathrm{d}s = \mathrm{d}^2({}^{t}q)/\mathrm{d}^2s = \rho\,{}^{t}e$ (ρ is the radius of curvature) is perpendicular to the tangent vector t_τ, and ${}^{t}e$ is known as unit normal vector,

$$ {}^{t}e = [e_x\ e_y\ e_z\ 0]^{\mathrm{T}} = \frac{1\mathrm{d}^2({}^{t}q)}{\rho\ \mathrm{d}^2s} = \frac{({}^{t}q' \times {}^{t}q'') \times {}^{t}q'}{|{}^{t}q' \times {}^{t}q''||{}^{t}q'|} \tag{3} $$

$$ = \left[\frac{-z'(h)}{\sqrt{x'(h)^2 + z'(h)^2}}\ 0\ \frac{x'(h)}{\sqrt{x'(h)^2 + z'(h)^2}}\ 0\right]^{\mathrm{T}} $$

Note that the appropriate sign must be chosen so that the outward normal can be obtained in this notation. Consequently, the unit normal ${}^{t}n$ at the point ${}^{t}r$ along the working surface is given by:

$$ {}^{t}n = [n_x\ n_y\ n_z\ 0]^{\mathrm{T}} = \mathrm{Rot}(z,v)\,{}^{t}e $$

$$ = \left[\frac{-z'(h)\mathrm{C}v}{\sqrt{x'(h)^2 + z'(h)^2}}\right. \tag{4} $$

$$ \left.\frac{-z'(h)\mathrm{S}v}{\sqrt{x'(h)^2 + z'(h)^2}}\ \frac{x'(h)}{\sqrt{x'(h)^2 + z'(h)^2}}0\right]^{\mathrm{T}} $$

Note that according to geometrics, any vector obtained by rotating tangent vector t_τ about its unit normal ${}^{t}e$ at an angle $\omega(0<\omega<2\pi)$ is also one of the unit tangent vectors ${}^{t}\varepsilon$ at point ${}^{t}q$ in 3D space. This leads to:

$$ {}^{t}\varepsilon = $$

$$ \begin{bmatrix} e_x^2(1-C\omega) + C\omega & e_ye_x(1-C\omega) - e_zS\omega & e_ze_x(1-C\omega) + e_yS\omega & 0 \\ e_xe_y(1-C\omega) + e_zS\omega & e_y^2(1-C\omega) + C\omega & e_ze_y(1-C\omega) - e_xS\omega & 0 \\ e_xe_z(1-C\omega) - e_yS\omega & e_ye_z(1-C\omega) + e_xS\omega & e_z^2(1-C\omega) + C\omega & 0 \\ 0 & 0 & 0 & 1 \end{bmatrix} $$

$$ \begin{bmatrix} \tau_x \\ \tau_y \\ \tau_z \\ 0 \end{bmatrix} \tag{5} $$

Further simplification of Eq. (5) is possible by utilizing the equations ${}^{t}eX{}^{t}\tau = j$ and ${}^{t}e.{}^{t}\tau = e_x\tau_x + e_z\tau_z = 0$, which results in:

$$ {}^{t}\varepsilon = [\tau_x\mathrm{C}\omega\ \mathrm{S}\omega\ \tau_z\mathrm{C}\omega\ 0]^{\mathrm{T}} \tag{6} $$

$$ = \left[\frac{x'(h)\mathrm{C}\omega}{\sqrt{x'(h)^2 + z'(h)^2}}\ \mathrm{S}\omega\ \frac{z'(h)\mathrm{C}\omega}{\sqrt{x'(h)^2 + z'(h)^2}}0\right]^{\mathrm{T}} $$

Consequently, in 3D space, any unit tangent vector ${}^{t}t$ at the point ${}^{t}r$ on the revolution working surface can be written as:

$$ {}^{t}t = \mathrm{Rot}(z,v)\,{}^{t}\varepsilon = \begin{bmatrix} t_x \\ t_y \\ t_z \\ 0 \end{bmatrix} \tag{7} $$

$$ = \begin{bmatrix} \dfrac{x'(h)\mathrm{C}\omega\mathrm{C}v}{\sqrt{x'(h)^2 + z'(h)^2}} - \mathrm{S}\omega\mathrm{S}v \\ \dfrac{x'(h)\mathrm{C}\omega\mathrm{S}v}{\sqrt{x'(h)^2 + z'(h)^2}} + \mathrm{S}\omega\mathrm{C}v \\ \dfrac{z'(h)\mathrm{C}\omega}{\sqrt{x'(h)^2 + z'(h)^2}} \\ 0 \end{bmatrix} $$

Table 1
Generating curves of grinding tool working surfaces

Working surface		$x(h)$	$z(h)$
Quadratic	Conical	h	$-mh$
	Elliptical	h	$\frac{b\sqrt{a^2-h^2}}{a}$
	Hyperbolic	h	$\frac{-b\sqrt{h^2-a^2}}{a}$
	Parabolic	h	$-ah^2$
Ball end milling cutter		$r\mathrm{S}(h/r)\ \ 0 < h < 0.5r\pi r\ \ 0.5\pi < h$	$-r\mathrm{C}(h/r)\ \ 0 < h < 0.5r\pi h-0.5r\pi\ \ 0.5r\pi < h$

$a > 0$ and $b > 0$

Eqs. (1), (3) and (7) give the parametric expression of a working surface of arbitrary revolution shape, and its unit normals and unit tangent vectors with respect to the tool frame $(xyz)_t$. Table 1 lists five generating curves ${}^tq$ of four different quadratic form-grinding tools and one axial-type tool. Once having these expressions, it is possible to determine the drill flute surfaces by conjugate surface theory and the drill flank surfaces by coordinate transformation.

3. Drill flute surfaces

In order to determine the flute surfaces of a drill with n flutes in terms of the motions of disk or axial-type tools (see Fig. 2) by using conjugate surface theory [22], one needs to define a drill coordinate frame $(xyz)_o$ to describe its position and orientation. The relative relation of $(xyz)_t$ built in tool with respect to drill frame $(xyz)_o$, when the tool generates the ith flute surface, can be obtained according to its generation motion, given as

$$
{}^{\circ}A_{t'i} = \mathrm{Rot}(x,180^{\circ})\mathrm{Trans}(0,0,a_z)\mathrm{Rot}
$$

$$
(z,\theta_i = \Omega t + 360^{\circ}(i-1)/n)\mathrm{Trans}(a_x,0,0)\mathrm{Rot}(x,\lambda)\mathrm{Rot}(y,\alpha) \qquad (8)
$$

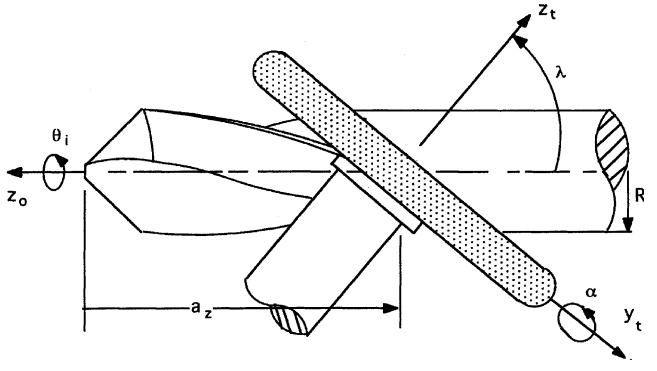

Fig. 2. Cutting the helical groove of a multiflute twist drill.

$$
= \begin{bmatrix}
\mathrm{C}\theta_i\mathrm{C}\alpha-\mathrm{S}\theta_i\mathrm{S}\lambda\mathrm{S}\alpha & -\mathrm{S}\theta_i\mathrm{C}\lambda & \mathrm{C}\theta_i\mathrm{S}\alpha+\mathrm{S}\theta_i\mathrm{S}\lambda\mathrm{C}\alpha & a_x\mathrm{C}\theta_i \\
-\mathrm{S}\theta_i\mathrm{C}\alpha-\mathrm{C}\theta_i\mathrm{S}\lambda\mathrm{S}\alpha & -\mathrm{C}\theta_i\mathrm{C}\lambda & -\mathrm{S}\theta_i\mathrm{S}\alpha+\mathrm{C}\theta_i\mathrm{S}\lambda\mathrm{C}\alpha & -a_x\mathrm{S}\theta_i \\
\mathrm{C}\lambda\mathrm{S}\alpha & -\mathrm{S}\lambda & -\mathrm{C}\lambda\mathrm{C}\alpha & -a_z \\
0 & 0 & 0 & 1
\end{bmatrix}
$$

where $\mathrm{Trans}(a_x,a_y,a_z)$ is the transformation corresponding to translation by a vector $a_xi + a_yj + a_zk$, and $\mathrm{Rot}(x,\lambda)$ and $\mathrm{Rot}(y,\alpha)$ are the rotation transformation matrices about the x and y axes given by (A2–A4 in the Appendix [21]. α and λ define the required tool orientation in order to generate the desired flute shape (see Fig. 2). $360^{\circ}(i-1)/n$ gives the initial angular position of the tool in order to produce the ith flute. The tool rotates with an angular velocity Ω and, at the same time, advances along the z and x axes of drill frame $(xyz)_o$ with position defined by $a_z = k_3\Omega t + mt$ and $a_x = a_{xo} + k_1\Omega t$, respectively. Note that $a_z = k_3\Omega t$ generates a helical flute and $a_z = mt$ generates a straight flute. Also note that a_x increases when the grinding tool advances along the shank, so that the web gradually increases in thickness towards the shank to give the drill strength (see Fig. 3). The flute surface is generated according to the conjugate surface theory. This theory states that these two surfaces have common point and common normal vector at the conjugate points. Based on this, conjugate points and the complete flute-profile can be determined from:

$$
n_i^{\mathrm{T}}\frac{\mathrm{d}(r_i)}{\mathrm{d}t} = ({}^{\circ}A_{t'i}\,{}^tn)^{\mathrm{T}}\frac{\mathrm{d}({}^{\circ}A_{t'i}\,{}^tr)}{\mathrm{d}t} = 0 \qquad (9)
$$

where r_i and n_i are, respectively, surface equation and unit outward normal with respect to frame $(xyz)_o$ obtained from the coordinate transformations by $r_i = {}^{\circ}A_{t'i}\,{}^tr_i$ and $n_i = {}^{\circ}A_{t'i}\,{}^tn$. Eq. (9) states that for continuous contact to be maintained between two moving surfaces, the relative sliding velocity $\mathrm{d}(r_i)/\mathrm{d}t$ must be orthogonal to the common normal n_i at the conjugate point. If this

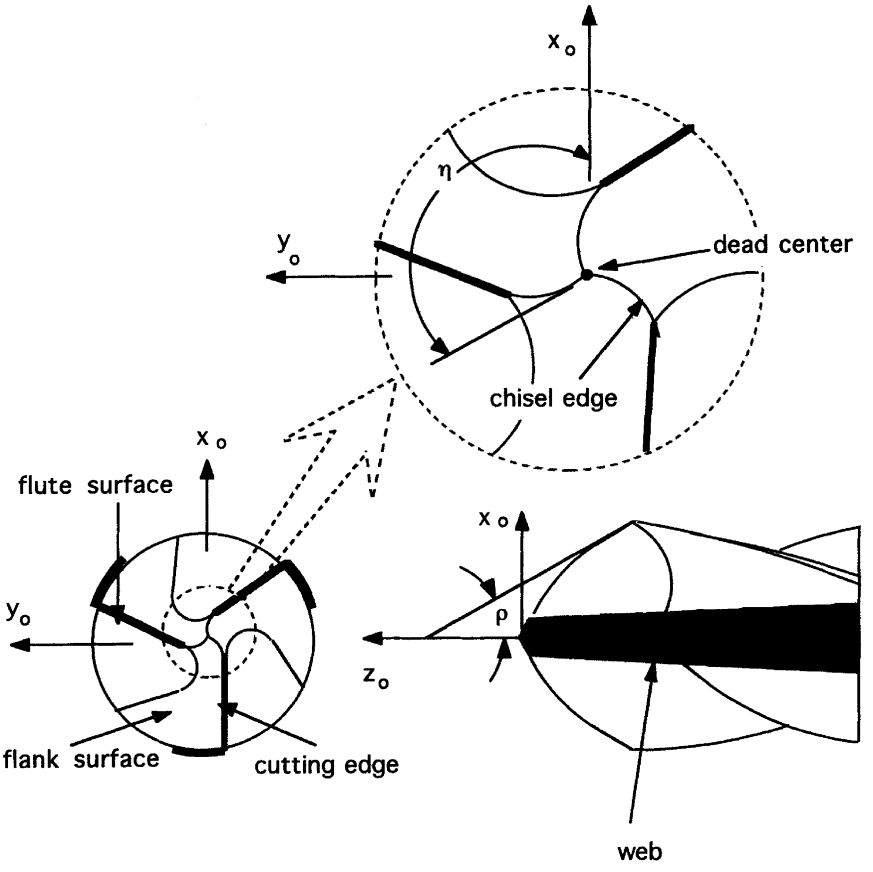

Fig. 3. A three fluted twist drill.

condition is not satisfied, then either the contact between the surfaces breaks or gouging occurs. If Eq. (9) is imposed on Eqs. (1) and (4), one can find the relation of the parameters h and v (denoted as $\bar{h}$ and $\bar{v}$, respectively) at the conjugate point expressed as

$$\begin{aligned}&\{-[x(\bar{h})x'(\bar{h}) + z(\bar{h})z'(\bar{h})]\Omega S\lambda - z'(\bar{h})\Omega(a_x S\lambda S\alpha\\&+ k_1 C\alpha - k_3 C\lambda S\alpha) + mz'(\bar{h})C\lambda S\alpha\}C\bar{v}\\&-\{[x(\bar{h})x'(\bar{h}) + z(\bar{h})z(\bar{h})]\Omega C\lambda S\alpha\\&+ z'(\bar{h})\Omega(a_x C\lambda + k_3 S\lambda) + mz'(\bar{h})S\lambda\}S\bar{v}\\&-x'(\bar{h})\Omega(a_x S\lambda C\alpha - k_1 S\alpha - k_3 C\lambda C\alpha)\\&+ mx'(\bar{h})C\lambda C\alpha = 0\end{aligned} \tag{10}$$

For a particular value of $\bar{h}$, which represents a point ${}^{t}q$ on the generating curve, a value of $\bar{v}$ can be found from the above equation. Now the ith flute surface $r_{\text{flute},i}$ generated by the tool can be obtained by substituting Eq. (10) into Eq. (1), and then transforming to frame $(xyz)_o$ by $r_{\text{flute},i} = {}^{\circ}A_{t'i}\,{}^{t}r$

$$r_{\text{flute},i} = [r_{ix}\ r_{iy}\ r_{iz}\ 1]^{\mathrm{T}} = \tag{11}$$

$$\begin{bmatrix} x(\bar{h})(C\theta_i C\alpha - S\theta_i S\lambda S\alpha)C\bar{v} - x(\bar{h})S\theta_i C\lambda S\bar{v} + z(\bar{h})(C\theta_i S\alpha + S\theta_i S\lambda C\alpha) + (a_{xo} + k_1\Omega t)C\theta_i \\ -x(\bar{h})(S\theta_i C\alpha + C\theta_i S\lambda S\alpha)C\bar{v} - x(\bar{h})C\theta_i C\lambda S\bar{v} + z(\bar{h})(-S\theta_i S\alpha + C\theta_i S\lambda C\alpha) - (a_{xo} + k_1\Omega t)S\theta_i \\ x(\bar{h})C\lambda S\alpha C\bar{v} - x(\bar{h})S\lambda S\bar{v} - z(\bar{h})C\lambda C\alpha - k_3\Omega t - mt \\ 1 \end{bmatrix}$$

The cross-sectional shape of the drill as intersected by a transverse plane normal to the drill axis at a particular z_t coordinate (say, $-z_t$), can be obtained by solving for t and $\bar{v}$ for a given $\bar{h}$ from the two nonlinear equations, $r_{iz} = -z_t$ and Eq. (10). The valid range of $\bar{v}$, $\pi/2 < \bar{v}_{\min} \leqslant \bar{v} \leqslant \bar{v}_{\max} < 3\pi/2$), (see Fig. 2) can be also obtained from $r_{ix}^2 + r_{iy}^2 = R^2$ (R is the radius of drill blank) during this iteration calculations.

The unit outward normal $n_{\text{flute},i}$ and unit tangent vector $t_{\text{flute},i}$ of the ith drill flute surface, which are two important parameters for determining the drill angles, are respectively given by

$$n_{\text{flute},i} = {}^{\circ}A_{t'i}\,{}^{t}n = [n_{ix}\ n_{iy}\ n_{iz}\ 0]^{\mathrm{T}} = \frac{1}{\sqrt{x'(\bar{h})^2 + z'(\bar{h})^2}} \tag{12}$$

$$\begin{bmatrix} -z'(\bar{h})C\bar{v}(C\theta_i C\alpha - S\theta_i S\lambda S\alpha) + z'(\bar{h})S\bar{v}S\theta_i C\lambda + x'(\bar{h})(C\theta_i S\alpha + S\theta_i S\lambda C\alpha) \\ z'(\bar{h})C\bar{v}(S\theta_i C\alpha + C\theta_i S\lambda S\alpha) + z'(\bar{h})S\bar{v}C\theta_i C\lambda + x'(\bar{h})(-S\theta_i S\alpha + C\theta_i S\lambda C\alpha) \\ -z'(\bar{h})C\bar{v}C\lambda S\alpha + z'(\bar{h})S\bar{v}S\lambda - x'(\bar{h})C\lambda C\alpha \\ 0 \end{bmatrix}$$

$$t_{\text{flute},i} = {}^{\circ}A_{t'i}\,{}^{t}t = [t_{ix}\ t_{iy}\ t_{iz}\ 0]^{\mathrm{T}} = \frac{C\omega}{\sqrt{x'(\bar{h})^2 + z'(\bar{h})^2}}$$

$$\begin{bmatrix} x'(\bar{h})C\bar{v}(C\theta_i C\alpha - S\theta_i S\lambda S\alpha) - x'(\bar{h})S\bar{v}S\theta_i C\lambda + z'(\bar{h})(C\theta_i S\alpha + S\theta_i S\lambda C\alpha) \\ -x'(\bar{h})C\bar{v}(S\theta_i C\alpha + C\theta_i S\lambda S\alpha) - x'(\bar{h})S\bar{v}C\theta_i C\lambda + z'(\bar{h})(-S\theta_i S\alpha + C\theta_i S\lambda C\alpha) \\ x'(\bar{h})C\bar{v}C\lambda S\alpha - x'(\bar{h})S\bar{v}S\lambda - z'(\bar{h})C\lambda C\alpha \\ 0 \end{bmatrix} \tag{13}$$

$$+ S\omega \begin{bmatrix} -S\bar{v}(C\theta_i C\alpha - S\theta_i S\lambda S\alpha) - C\bar{v}S\theta_i C\lambda \\ S\bar{v}(S\theta_i C\alpha + C\theta_i S\lambda S\alpha) - C\bar{v}C\theta_i C\lambda \\ -S\bar{v}C\lambda S\alpha - C\bar{v}S\lambda \\ 0 \end{bmatrix}$$

Since $\bar{v}$ and $\bar{h}$ are related through Eq. (10), we can say that the ith flute surface $r_{\text{flute},i}$, unit outward normal $n_{\text{flute},i}$, and unit tangent vector $t_{\text{flute},i}$ can be expressed solely in terms of $\bar{h}$ and θ_i for a given tool and $a_x, a_z, \lambda, \alpha$. Fig. 4 gives the transverse section of a three-fluted drill at $r_{iz} = -10$ (all length units used hereafter are mm) produced by a disk-type grinding tool having the following generating curve

$$\begin{cases} x(h) = 40 & 0 \le h \le 40 \\ x(h) = 40 + 3.5S\left(\dfrac{h-40}{3.5}\right) & 40 < h < 40 + 3.5\pi \\ x(h) = 80 + 3.5\pi - h & 40 + 3.5\pi \le h \le 80 + 3.5\pi \end{cases} \tag{14}$$

$$\begin{cases} z(h) = 3.5 & 0 \le h \le 40 \\ z(h) = 3.5C\left(\dfrac{h-40}{3.5}\right) & 40 < h < 40 + 3.5\pi \\ z(h) = -3.5 & 40 + 3.5\pi \le h \le 80 + 3.5\pi \end{cases}$$

The employed parameters are $\alpha = 10^\circ$, $\lambda = 38^\circ$, $R = 15$, $a_{xo} = 45.5$, $k_1 = 0.286$, $k_3 = 19.098$, $m = 0$. From numerical calculations, the ranges of $\bar{v}$ and $\bar{h}$ on the transverse plane normal at $r_{iz} = -10$ are respectively given by $154.43^\circ \le \bar{v} \le 193.00^\circ$, $41.89 \le \bar{h} \le 50.44$.

4. Tool flank surfaces

The following will discuss a drill shape with various flank surfaces as produced by various grinding tools. In order to obtain an expression for a drill flank as produced by a given grinding tool, the generating curve of the form-grinding tool should first be defined as ${}^t q = [h_i \; 0 \; f(h_i) \; 1]^T$. The grinding tool's working surface, unit outward normal and unit tangent vector are then obtained respectively from Eqs. (1), (4) and (7) as

$${}^t r = [h_i C v_i \; h_i S v_i \; f(h)_i \; 1]^T \tag{15}$$

$${}^t n = \left[\frac{-f'(h_i) C v_i}{\sqrt{1 + f'(h_i)^2}} \; \frac{-f'(h_i) S v_i}{\sqrt{1 + f'(h_i)^2}} \; \frac{1}{\sqrt{1 + f'(h_i)^2}} \; 0 \right]^T \tag{16}$$

$${}^t t = \left[\frac{C\omega i C v_i}{\sqrt{1 + f'(h_i)^2}} - S\omega_i S v_i \; \frac{C\omega_i S v_i}{\sqrt{1 + f'(h_i)^2}} + S\omega_i C v_i \; \frac{f'(h_i) C\omega_i}{\sqrt{1 + f'(h_i)^2}} \; 0 \right]^T \tag{17}$$

Note that the tool profile described in Eq. (17) is not the tool used in machining the drill flutes. Also note that when grinding the drill flanks using form-grinding tools,

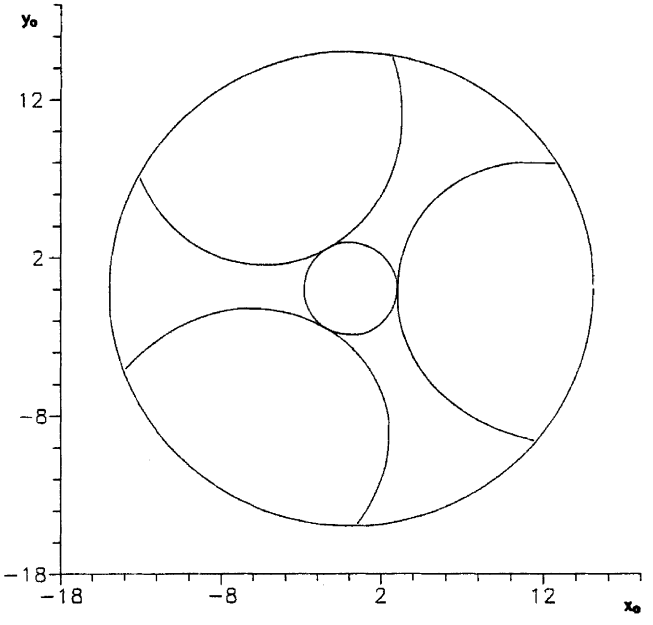

Fig. 4. The transverse section of a three-fluted drill at r_{iz}=10 mm.

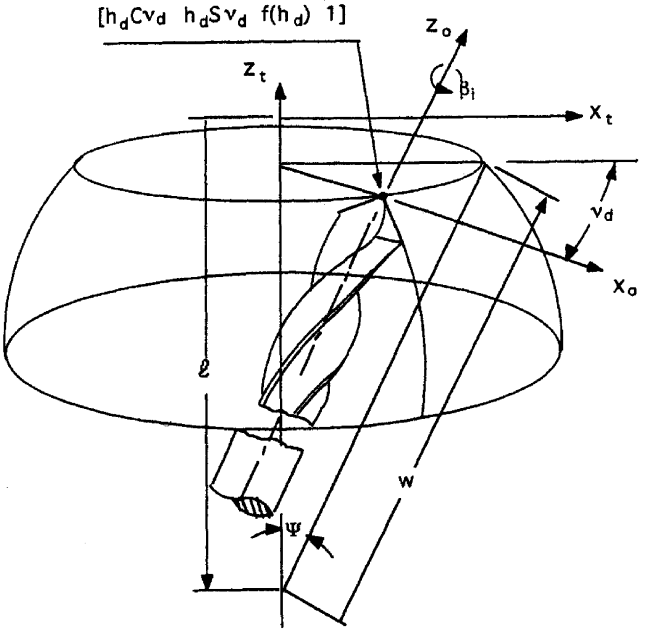

Fig. 5. Grinding of drill flank surfaces by using form-grinding tool.

the drill flank axiomatically must lie along the working surface of the tool (see Fig. 5) by the following movement procedure.

It is well known that three independent rotation angles and three independent translation components are needed in 3D space to completely specify the orientation and position of a rigid body. Note that the working surface of the grinding tool is surface of revolution. Therefore, only two positive angles (ψ and β) are required to describe the rotational orientation of the drill relative to the form-grinding tool, while three positive translations (g, ℓ, and w) are required to shift the drill's origin. Note that these n drill flanks are symmetrical with respect to the drill axis. Consequently, one can rotate the drill an extra angle $360°(i-1)/n$ about drill's axis to machine the ith flank surface. Consequently, in order to generate the ith flank surface the relative configuration of the drill's frame with respect to the tool's frame can be obtained by the following movement

$$
\begin{aligned}
&{}^{t}\Lambda_{o'i} = \mathrm{Trans}(0,0,-\ell)\mathrm{Rot}(y,\Psi)\mathrm{Trans}(0,0,w)\\
&\mathrm{Trans}(0,-g,0)\mathrm{Rot}(z,\beta_i = \beta + 360°(i-1)/n)\\
&= \begin{bmatrix} C\Psi C\beta_i & -C\Psi S\beta_i & S\Psi & wS\Psi \\ S\beta_i & C\beta_i & 0 & -g \\ -S\Psi C\beta_i & S\Psi S\beta_i & C\Psi & wC\Psi-\ell \\ 0 & 0 & 0 & 1 \end{bmatrix}
\end{aligned} \tag{18}
$$

The value of β is usually determined by setting the cutting edges as nearly straight for a given flute shape. One must note that when flank surfaces are produced, in order to keep the dead center at the origin of frame $(xyz)_o$, the origin of frame $(xyz)_o$ must be on the working surface of the form-grinding tool. In other words, the fourth column of Eq. (18) should be coincides with one point (denoted as $[h_d C\nu_d \; h_d S\nu_d \; f(h_d) \; 1]^T$) of the working surfaces. As a result, there are two constraints between these five parameters

$$\mathrm{Tan}(\nu_d) = \frac{-g}{w S\Psi} \tag{19}$$

$$\ell = wC\Psi - f\left(\sqrt{w^2S^2\Psi + g^2}\right) \tag{20}$$

Eq. (19) states that coordinates of $-g$ and $wS\Psi$ have to be one point of the generating curve defined by angle ν_d. Finally, the ith flank surface in the drill frame $(xyz)_o$ can be obtained by transforming the grinding tool working surface, Eq. (15), to frame $(xyz)_o$ by $R_{\mathrm{flank},i} = {}^{\circ}\Lambda_{t'i}\,{}^{t}r$, where ${}^{\circ}\Lambda_{t'i}$ is the relative configuration of the form-grinding tool frame $(xyz)_t$ with respect to drill frame $(xyz)_o$ given by (see Eq. (18))

$$
\begin{aligned}
&{}^{\circ}\Lambda_{t'i} = ({}^{t}\Lambda_{o'i})^{-1} = \mathrm{Rot}(z,-\beta_i)\;\mathrm{Trans}(0,g,0)\\
&\mathrm{Trans}(0,0,-w)\mathrm{Rot}\;(y,-\Psi)\mathrm{Trans}(0,0,\ell)
\end{aligned} \tag{21}
$$

$$
\begin{aligned}
&= \begin{bmatrix} C\Psi C\beta_i & S\beta_i & -S\Psi C\beta_i & -\ell C\beta_i S\Psi + gS\beta_i \\ -C\Psi S\beta_i & C\beta_i & S\Psi S\beta_i & \ell S\beta_i S\Psi + gC\beta_i \\ S\Psi & 0 & C\Psi & \ell C\Psi - w \\ 0 & 0 & 0 & 1 \end{bmatrix}\\
&R_{\mathrm{flank},i} = {}^{\circ}\Lambda_{t,i}\,{}^{t}r = \begin{bmatrix} R_{ix} \\ R_{iy} \\ R_{iz} \\ 1 \end{bmatrix}
\end{aligned} \tag{22}
$$

$$= \begin{bmatrix} h_i[C\beta_i C\Psi C\nu_i + S\beta_i S\nu_i] - [f(h_i) + \ell]C\beta_i S\Psi + gS\beta_i \\ h_i[-S\beta_i C\Psi C\nu_i + C\beta_i S\nu_i] + [f(h_i) + \ell]S\beta_i S\Psi + gC\beta_i \\ h_i S\Psi C\nu_i + [f(h_i) + \ell]C\Psi - w \\ 1 \end{bmatrix}$$

As can be seen from Eq. (22), the geometry of the ith drill flank surface varies continuously as function of Ψ, h_i, g, w and ℓ. Hence, the rotational orientation and translations of the drill are important factors determining the drill characteristics.

The unit outward normal $N_{\mathrm{flank},i}$ and unit tangent vector $T_{\mathrm{flank},i}$ of the flanks are two important vectors determining drill point angle, clearance angle and chisel edge angle. They are respectively given by transforming Eqs. (16) and (17) to frame $(xyz)_o$ as

$$
\begin{aligned}
&N_{\mathrm{flank},i} = {}^{\circ}\Lambda_{t'i}\,{}^{t}n\\
&= \begin{bmatrix} N_{ix} \\ N_{iy} \\ N_{iz} \\ 0 \end{bmatrix} = \frac{1}{\sqrt{1 + f'(h_i)^2}}
\end{aligned} \tag{23}
$$

$$\begin{bmatrix} -f'(h_i)[C\beta_i C\Psi C\nu_i + S\beta_i S\nu_i] - C\beta_i S\Psi \\ -f'(h_i)[-S\beta_i C\Psi C\nu_i + C\beta_i S\nu_i] + S\beta_i S\Psi \\ -f'(h_i)S\Psi C\nu_i + C\Psi \\ 0 \end{bmatrix}$$

$$
\begin{aligned}
&T_{\mathrm{flank},i} = {}^{\circ}\Lambda_{t,i}\,{}^{t}t = [T_{ix}\; T_{iy}\; T_{iz}\; 0]^T\\
&= \frac{C\omega_i}{\sqrt{1 + f'(h_i)^2}} \begin{bmatrix} C\beta_i C\Psi C\nu_i + S\beta_i S\nu_i - f'(h_i)C\beta_i S\Psi \\ -S\beta_i C\Psi C\nu_i + C\beta_i S\nu_i + f'(h_i)S\beta_i S\Psi \\ S\Psi C\nu_i + f'(h_i)C\Psi \\ 0 \end{bmatrix}
\end{aligned} \tag{24}
$$

$$+ S\omega_i \begin{bmatrix} -C\beta_i C\Psi S\nu_i + S\beta_i C\nu_i \\ S\beta_i C\Psi S\nu_i + C\beta_i C\nu_i \\ -S\Psi S\nu_i \\ 0 \end{bmatrix}$$

Once having the expressions of flute and flank surfaces, and also their unit outward normals and unit tangent vectors, it is possible to investigate various characteristic angles of drill, as is done in the following sections.

5. Cutting edge and drill point angle

The ith cutting edge $\underline{R}_{edge,i}$ is formed by the intersection of the ith flank surface $R_{\text{flank},i}$ and the ith flute surface $r_{\text{flute},i}$. Numerical techniques are needed to determine or optimize these space curve edges by solving for flank variables v_i and h_i, and flute variables $\bar{v}$ and θ_i for a given $\bar{h}$ (denoted as $\underline{v}_i,\underline{h}_i,\underline{\bar{v}},\underline{\theta}_i$ and $\underline{\bar{h}}$ respectively) by using conjugate Eq. (10) and setting $R_{\text{flank},i} = r_{\text{flute},i}$. Therefore, the ith cutting edge is obtained from Eq. (22) as

$$\underline{R}_{\text{edge},i} = \begin{bmatrix} \underline{R}_{ix} \\ \underline{R}_{iy} \\ \underline{R}_{iz} \\ 1 \end{bmatrix} \tag{25}$$

$$= \begin{bmatrix} \underline{h}_i(\mathrm{C}\beta_i\mathrm{C}\Psi\mathrm{C}\underline{v}_i + \mathrm{S}\beta_i\mathrm{S}\underline{v}_i) - [f(\underline{h}_i) + \ell]\mathrm{C}\beta_i\mathrm{S}\Psi + g\mathrm{S}\beta_i \\ \underline{h}_i(-\mathrm{S}\beta_i\mathrm{C}\Psi\mathrm{C}\underline{v}_i + \mathrm{C}\beta_i\mathrm{S}\underline{v}_i) + [f(\underline{h}_i) + \ell]\mathrm{S}\beta_i\mathrm{S}\Psi + g\mathrm{C}\beta_i \\ \underline{h}_i\mathrm{S}\Psi\mathrm{C}\underline{v}_i + [f(\underline{h}_i) + \ell]\mathrm{C}\Psi - w \\ 1 \end{bmatrix}$$

Fig. 6 shows the front end view of the major cutting edges of a drill having the flute shapes shown in cross-section in Fig. 4, while the generating curve of the form-grinding tool is ${}^{t}q = [h_i \;\; 0 \;\; -1.73h_i \;\; 1]^{\mathrm{T}}$ and parameters used are $\Psi = 29^{\circ}$, $g = 8.205$, $w = 87.065$, $\ell = 150.627$ and $\beta = 38^{\circ}$

In order to determine the rake and clearance angles, The normals along the cutting edges at both flute and flank surfaces from Eqs. (12) and (23) are required:

$$\underline{n}_{\text{edge at flute},i} = [\underline{n}_{ix}\;\underline{n}_{iy}\;\underline{n}_{iz}\;o]^{\mathrm{T}} = \frac{1}{\sqrt{x'(\bar{h})^2 + z'(\bar{h})^2}} \tag{26}$$

$$\begin{bmatrix} -z'(\bar{h})\mathrm{C}\bar{v}(\mathrm{C}\underline{\theta}_i\mathrm{C}\alpha - \mathrm{S}\underline{\theta}_i\mathrm{S}\lambda\mathrm{S}\alpha) + z'(\bar{h})\mathrm{S}\bar{v}\mathrm{S}\underline{\theta}_i\mathrm{C}\lambda + x'(\bar{h})(\mathrm{C}\underline{\theta}_i\mathrm{S}\alpha + \mathrm{S}\underline{\theta}_i\mathrm{S}\lambda\mathrm{C}\alpha) \\ z'(\bar{h})\mathrm{C}\bar{v}(\mathrm{S}\underline{\theta}_i\mathrm{C}\alpha + \mathrm{C}\underline{\theta}_i\mathrm{S}\lambda\mathrm{S}\alpha) + z'(\bar{h})\mathrm{S}\bar{v}\mathrm{C}\underline{\theta}_i\mathrm{C}\lambda + x'(\bar{h})(-\mathrm{S}\underline{\theta}_i\mathrm{S}\alpha + \mathrm{C}\underline{\theta}_i\mathrm{S}\lambda\mathrm{C}\alpha) \\ -z'(\bar{h})\mathrm{C}\bar{v}\mathrm{C}\lambda\mathrm{S}\alpha + z'(\bar{h})\mathrm{S}\bar{v}\mathrm{S}\lambda - x'(\bar{h})\mathrm{C}\lambda\mathrm{C}\alpha \\ 0 \end{bmatrix}$$

$$\underline{\mathrm{N}}_{\text{edge at flank},i} = \begin{bmatrix} \underline{\mathrm{N}}_{ix} \\ \underline{\mathrm{N}}_{iy} \\ \underline{\mathrm{N}}_{iz} \\ 0 \end{bmatrix} = \frac{1}{\sqrt{1 + f'(h_i)^2}} \tag{27}$$

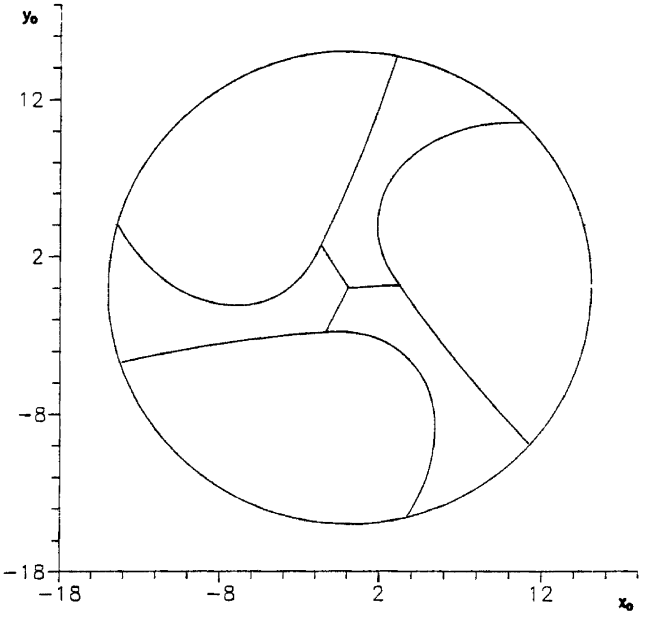

Fig. 6. The front view of the major cutting edges of a three-fluted drill.

$$\begin{bmatrix} -f'(\underline{h}_i)[\mathrm{C}\beta_i\mathrm{C}\Psi\mathrm{C}\underline{v}_i + \mathrm{S}\beta_i\mathrm{S}\underline{v}_i] - \mathrm{C}\beta_i\mathrm{S}\Psi \\ -f'(\underline{h}_i)[-\mathrm{S}\beta_i\mathrm{C}\Psi\mathrm{C}\underline{v}_i + \mathrm{C}\beta_i\mathrm{S}\underline{v}_i] + \mathrm{S}\beta_i\mathrm{S}\Psi \\ -f'(\underline{h}_i)\mathrm{S}\Psi\mathrm{C}\underline{v}_i + \mathrm{C}\Psi \\ 0 \end{bmatrix}$$

Furthermore, one can obtain the common unit tangent vector (denoted as $\underline{\mathrm{T}}_{\text{edge},i}$) of $R_{\text{flank},i}$ and $r_{\text{flute},i}$ along $\underline{\mathrm{R}}_{\text{edge},i}$ by determining ω_i and ω (denoted as $\underline{\omega}_i$, and $\underline{\omega}$ respectively) from $T_{\text{flank},i} = t_{\text{flute},i}$. Therefore, one has the following unit tangent vector along the ith cutting edge

$$\underline{\mathrm{T}}_{\text{edge},i} = [\underline{\mathrm{T}}_{ix}\;\underline{\mathrm{T}}_{iy}\;\underline{\mathrm{T}}_{iz}\;0]^{\mathrm{T}} \tag{28}$$

$$= \frac{\mathrm{C}\underline{\omega}_i}{\sqrt{1 + f'(\underline{h}_i)^2}} \begin{bmatrix} \mathrm{C}\beta_i\mathrm{C}\Psi\mathrm{C}\underline{v}_i + \mathrm{S}\beta_i\mathrm{S}\underline{v}_i - f'(\underline{h}_i)\mathrm{C}\beta_i\mathrm{S}\Psi \\ -\mathrm{S}\beta_i\mathrm{C}\Psi\mathrm{C}\underline{v}_i + \mathrm{C}\beta_i\mathrm{S}\underline{v}_i + f'(\underline{h}_i)\mathrm{S}\beta_i\mathrm{S}\Psi \\ \mathrm{S}\Psi\mathrm{C}\underline{v}_i + f'(\underline{h}_i)\mathrm{C}\Psi \\ 0 \end{bmatrix}$$

$$+ \mathrm{S}\underline{\omega}_i \begin{bmatrix} -\mathrm{C}\beta_i\mathrm{C}\Psi\mathrm{S}\underline{v}_i + \mathrm{S}\beta_i\mathrm{C}\underline{v}_i \\ \mathrm{S}\beta_i\mathrm{C}\Psi\mathrm{S}\underline{v}_i + \mathrm{C}\beta_i\mathrm{C}\underline{v}_i \\ -\mathrm{S}\Psi\mathrm{S}\underline{v}_i \\ 0 \end{bmatrix}$$

The semi-included angle $\xi_{\text{edge},i}$ of the cutting edges is the angle between the tangent vector $\underline{\mathrm{T}}_{\text{edge},i}$ along the curved cutting edge and the drill axis z_o, and is given by

$$C\xi_{\text{edge},i} = [0\ 0\ -1\ 0]\underline{\underline{T}}_{\text{edge},i} = -\underline{\underline{T}}_{iz} = \frac{-C\underline{\underline{\omega}}_i}{\sqrt{1 + f'(\underline{\underline{h}}_i)^2}} + S\underline{\underline{\omega}}_i S\Psi S\underline{\underline{\nu}}_i \tag{29}$$

which is usually different at different points. Lin et al. [10] defined the semi-point angle as the acute angle between the tangent to the projection of the cutting edge at the outer corner and the drill axis z_o on the xz plane of frame $(xyz)_o$. Therefore, the point angle of the case shown in Fig. 6 is $2\xi_{\text{edge},i} = 116.1°$, evaluated at the outer corner.

6. Chisel edge and its angle

The chisel edge represents part of the intersection curve of two sequential flank surfaces. Its calculation again needs numerical techniques to determine the ith chisel edge (denoted as $\underline{\underline{R}}_{\text{chisel},i}$) by solving for variables ν_i, ν_{i+1} and h_{i+1} for a given h_i (denoted as $\underline{\underline{\nu}}_i$, $\underline{\underline{\nu}}_{i+1}$, $\underline{\underline{h}}_{i+1}$, and $\underline{\underline{h}}_i$ respectively) from $\underline{\underline{R}}_{\text{flank},i} = \underline{\underline{R}}_{\text{flank},i+1}$. Then the ith chisel edge $\underline{\underline{R}}_{\text{chisel},i}$ is obtained from Eq. (21):

$$\underline{\underline{R}}_{\text{chisel},i} = \begin{bmatrix} \underline{\underline{R}}_{ix} \\ \underline{\underline{R}}_{iy} \\ \underline{\underline{R}}_{iz} \\ 1 \end{bmatrix} \tag{30}$$

$$= \begin{bmatrix} \underline{\underline{h}}_i[C\beta_i C\Psi C\underline{\underline{\nu}}_i + S\beta_i S\underline{\underline{\nu}}_i] - [f(\underline{\underline{h}}_i) + \lambda]C\beta_i S\Psi + gS\beta_i \\ \underline{\underline{h}}_i[-S\beta_i C\Psi C\underline{\underline{\nu}}_i + C\beta_i S\underline{\underline{\nu}}_i] + [f(\underline{\underline{h}}_i) + \lambda]S\beta_i S\Psi + gC\beta_i \\ \underline{\underline{h}}_i S\Psi C\underline{\underline{\nu}}_i + [f(\underline{\underline{h}}_i) + \lambda]C\Psi - w \\ 1 \end{bmatrix}$$

Again, in order to investigate the rake and clearance angles of the chisel edges, one needs the normals on the flank surfaces $R_{\text{flank},i}$ and $R_{\text{flank},i+1}$ along the chisel edges from Eq. (23):

$$\underline{\underline{N}}_{\text{chisel on flank},i} = \begin{bmatrix} \underline{\underline{N}}_{ix} \\ \underline{\underline{N}}_{iy} \\ \underline{\underline{N}}_{iz} \\ 0 \end{bmatrix} = \frac{1}{\sqrt{1 + f'(\underline{\underline{h}}_i)^2}} \tag{31}$$

$$\begin{bmatrix} -f'(\underline{\underline{h}}_i)[C\beta_i C\Psi C\underline{\underline{\nu}}_i + S\beta_i S\underline{\underline{\nu}}_i] - C\beta_i S\Psi \\ -f'(\underline{\underline{h}}_i)[-S\beta_i C\Psi C\underline{\underline{\nu}}_i + C\beta_i S\underline{\underline{\nu}}_i] + S\beta_i S\Psi \\ -f'(\underline{\underline{h}}_i)S\Psi C\underline{\underline{\nu}}_i + C\Psi \\ 0 \end{bmatrix}$$

$$\underline{\underline{N}}_{\text{chisel on flank},i+1} = [\underline{\underline{N}}_{i+1x}\ \underline{\underline{N}}_{i+1y}\ \underline{\underline{N}}_{i+1z}\ 0]^{\mathrm{T}} = \frac{1}{\sqrt{1 + f'(\underline{\underline{h}}_{i+1})^2}} \tag{32}$$

$$\begin{bmatrix} -f'(\underline{\underline{h}}_{i+1})[C\beta_{i+1} C\Psi C\underline{\underline{\nu}}_{i+1} + S\beta_{i+1} S\underline{\underline{\nu}}_{i+1}] - C\beta_{i+1} S\Psi \\ -f'(\underline{\underline{h}}_{i+1})[-S\beta_{i+1} C\Psi C\underline{\underline{\nu}}_{i+1} + C\beta_{i+1} S\underline{\underline{\nu}}_{i+1}] + S\beta_{i+1} S\Psi \\ -f'(\underline{\underline{h}}_{i+1})S\Psi C\underline{\underline{\nu}}_{i+1} + C\Psi \\ 0 \end{bmatrix}$$

Furthermore, one can obtain the common unit tangent vector (denoted as $\underline{\underline{T}}$) along that ith chisel edge by determining ω_i and ω_{i+1} (denoted as $\underline{\underline{\omega}}_i$ and $\underline{\underline{\omega}}_{i+1}$ respectively) from $T_i = T_{i+1}$. The common unit tangent vector along the ith chisel edge is

$$\underline{\underline{T}}_{\text{chisel},i} = [\underline{\underline{T}}_{ix}\ \underline{\underline{T}}_{iy}\ \underline{\underline{T}}_{iz}\ 0]^{\mathrm{T}} = \frac{C\underline{\underline{\omega}}_i}{\sqrt{1 + f'(\underline{\underline{h}}_i)^2}}$$

$$\begin{bmatrix} [C\beta_i C\Psi C\underline{\underline{\nu}}_i + S\beta_i S\underline{\underline{\nu}}_i] - f'(\underline{\underline{h}}_i)C\beta_i S\Psi \\ [-S\beta_i C\Psi C\underline{\underline{\nu}}_i + C\beta_i S\underline{\underline{\nu}}_i] + f'(\underline{\underline{h}}_i)S\beta_i S\Psi \\ S\Psi C\underline{\underline{\nu}}_i + f'(\underline{\underline{h}}_i)C\Psi \\ 0 \end{bmatrix} \tag{33}$$

$$+ S\underline{\underline{\omega}}_i \begin{bmatrix} -C\beta_i C\Psi S\underline{\underline{\nu}}_i + S\beta_i C\underline{\underline{\nu}}_i \\ S\beta_i C\Psi S\underline{\underline{\nu}}_i + C\beta_i C\underline{\underline{\nu}}_i \\ -S\Psi S\underline{\underline{\nu}}_i \\ 0 \end{bmatrix}$$

The ith chisel edge angle $\eta_{\text{edge},i}$ of a multiflute drill is the acute angle between the tangent to the projection of that chisel edge at the drill point center ($\underline{\underline{\nu}}_i = \nu_d$ and $\underline{\underline{h}}_i = h_d$, see Fig. 5) and x_o axis onto a plane normal to the drill axis [10]. Lin expressed $\eta_{\text{edge},i}$ as

$$C\eta_{\text{edge},i} = \underline{\underline{T}}_x = \frac{C\underline{\underline{\omega}}_i[C\beta_i C\Psi C\nu_d + S\beta_i S\nu_d] - f'(h_d)C\beta_i S\Psi}{\sqrt{1 + f'(h_d)^2}} - S\underline{\underline{\omega}}_i[C\beta_i C\Psi S\nu_d - S\beta_i C\nu_d] \tag{34}$$

For the first chisel edge angle of the drill in Fig. 6, $\eta_{edge,1} = 79.72°$. The rake angle and clearance angle of chisel edges according to ISO standards will be discussed in the following section.

7. Rake angle and clearance angle

The geometry and nomenclature of drills are surprisingly complicated subjects. It is difficult to calculate or even discuss the appropriate planes in which the various

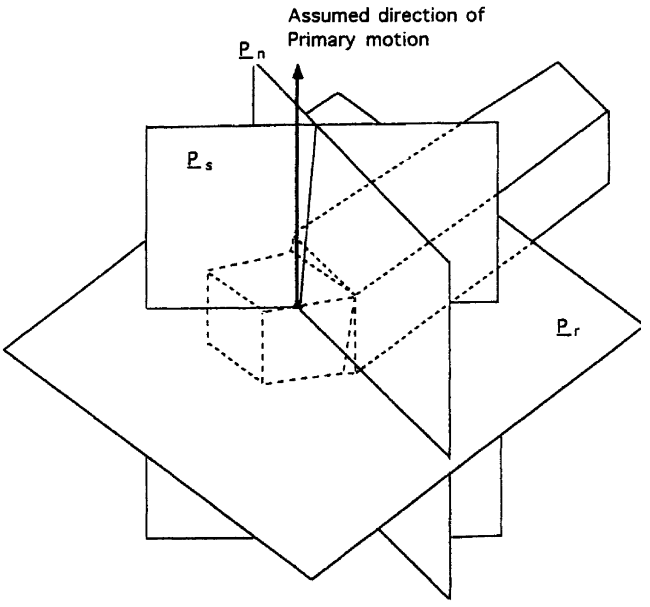

Fig. 7. Tool-in-hand planes for the major cutting edge.

angles of a drill should be measured because of confusion among current definitions. The international standard (ISO) recommendation [23] established two systems of planes, tool-in-use and tool-in-hand, that can be used to define the various angles of the face and flank of a single-point tool (see Fig. 7). The tool-in-use system is defined in relation to the resultant cutting direction. The tool-in-hand system, on the other hand, is defined in relation to the tool base and is used for the purposes of grinding and sharpening the tool. In this paper, the tool-in-hand system will be used here to define the required planes, which are the tool reference plane $\underline{P}_r$ (the plane perpendicular to the primary motion), the cutting edge plane $\underline{P}_s$ (the plane tangential to the cutting edge and perpendicular to the tool reference plane), and the cutting edge normal plane $\underline{P}_n$ (the plane perpendicular to the cutting edge) (see Fig. 7). Table 2 shows how the tool rake angle γ, clearance angle Σ, and wedge angle $\mu = 90° - \gamma - \Sigma$ are defined with respect to a selected point on the cutting edge by ISO.

In drilling, the primary motions of points along cutting edge and chisel edge are respectively given by $k \times \underline{R}_{\text{edge},i} = -\underline{R}_{iy}i + \underline{R}_{ix}j$ and $k \times \underline{R}_{\text{chisel},i} = -\underline{R}_{iy}i + \underline{R}_{ix}j$ where i, j and k are unit directions of drill frame $(xyz)_o$. Therefore, the unit normals of tool reference planes at all points on cutting edge and on chisel edge are given by $\not\angle_{\text{edge},i} = (-\underline{R}_{iy}i + \underline{R}_{ix}j)/\sqrt{\underline{R}_{ix}^2 + \underline{R}_{iy}^2}$ and $\not\angle_{\text{chisel},i} = (-\underline{R}_{iy}i + \underline{R}_{ix}j)/\sqrt{\underline{R}_{ix}^2 + \underline{R}_{iy}^2}$, respectively. By the definition of cutting edge plane $\underline{P}_s$, the unit normals of $\underline{P}_s$ at points on cutting edge and on chisel edge as $\underline{T}_{\text{edge},i} X \not\angle_{\text{edge},i}$ and $\underline{T}_{\text{chisel},i} X \not\angle_{\text{chisel},i}$ also can be obtained, respectively. Furthermore, from geometrics it is known that the angle δ between plane $\underline{P}_a$ and plane $\underline{P}_b$ measured in plane $\underline{P}_c$ is uniquely determined by the respective unit normals $\not\angle_a$, $\not\angle_b$, and $\not\angle_c$ as $C\delta = (\not\angle_a \times \not\angle_c).(\not\angle_c \times \not\angle_a)$ (see Fig. 8). By applying these conclusions and the Table 2 definitions, Table 3 presents the definitions of rake angle γ, clearance angle Σ and wedge angle μ along the ith cut-

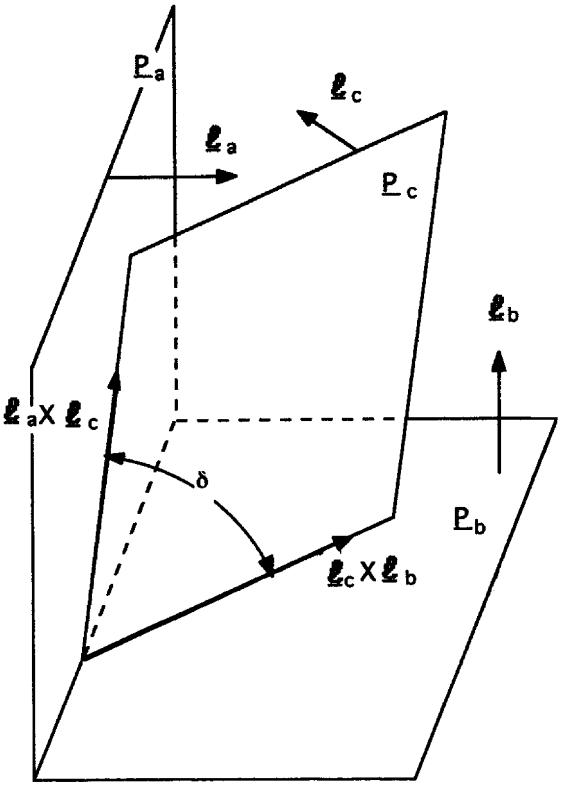

Fig. 8. The determination of angle between plane $\underline{P}_a$ and plane $\underline{P}_b$ measured in plane $\underline{P}_c$.

Table 2
Tool angle definitions from ISO

Angle	Is the angle between	And	Measured in plane
Tool rake angle γ	$\underline{P}_{\text{face}}$	$\underline{P}_{\text{r}}$	$\underline{P}_{\text{n}}$
Tool clearance angle Σ	$\underline{P}_{\text{flank}}$	$\underline{P}_{\text{s}}$	$\underline{P}_{\text{n}}$
Tool wedge angle μ	$\underline{P}_{\text{face}}$	$\underline{P}_{\text{flank}}$	$\underline{P}_{\text{n}}$

[a] $\underline{P}_{\text{face}}$: tool face plane
[b] $\underline{P}_{\text{flank}}$: tool flank plane

Table 3
Determination of various drill angles

Angle		Is the angle between	And	Measured in plane
Cutting edge	Rake angle γ_{edge}	$\underline{n}_{edge\ on\ flute,i}$	$\measuredangle_{edge,i}$	$\underline{T}_{edge,i}$
	Clearance angle Σ_{edge}	$\underline{N}_{edge\ on\ flank,i}$	$\underline{T}_{edge,i} \times \measuredangle_{edge,i}$	$\underline{T}_{edge,i}$
	Wedge angle μ_{edge}	$\underline{n}_{edge\ on\ flute,i}$	$\underline{N}_{edge\ on\ flank,i}$	$\underline{T}_{edge,i}$
Chisel edge	Rake angle γ_{chisel}	$\underline{\underline{N}}_{flank,i}$	$\measuredangle_{chisel,i}$	$\underline{\underline{T}}_{chisel,i}$
	Clearance angle Σ_{chisel}	$\underline{\underline{N}}_{flank,i+1}$	$\underline{\underline{T}}_{chisel,i} \times \measuredangle_{chisel,i}$	$\underline{\underline{T}}_{chisel,i}$
	Wedge angle μ_{chisel}	$\underline{\underline{N}}_{flank,i}$	$\underline{\underline{N}}_{flank,i+1}$	$\underline{\underline{T}}_{chisel,i}$

ting edge and the ith chisel edge in terms of the unit normals of various planes.

Fig. 9 gives the rake angle $\gamma_{edge,i}$ and clearance angle $\Sigma_{edge,i}$ of points along the first cutting edge. The main defect of a standard twist drill is the very large negative rake angle on the part of the cutting edge close to the drill core, which greatly increases the deformation of metal chips and the cutting force during a drilling operation. The ranges of rake angle $\gamma_{chisel,i}$, clearance angle $\Sigma_{chisel,i}$ and wedge angle $\mu_{chisel,i}$ along the first chisel edge are respectively given by $-64.04^\circ \le \gamma_{chisel,i} \le -62.93^\circ$, $25.08^\circ \le \Sigma_{chisel,i} \le 26.92^\circ$ and $126.01^\circ \le \mu_{chisel,i} \le 128.96^\circ$. One feature of three-fluted drills is the large negative rake angles on the chisel edges. This can be easily simulated by using a pyramid sitting on the drill's core.

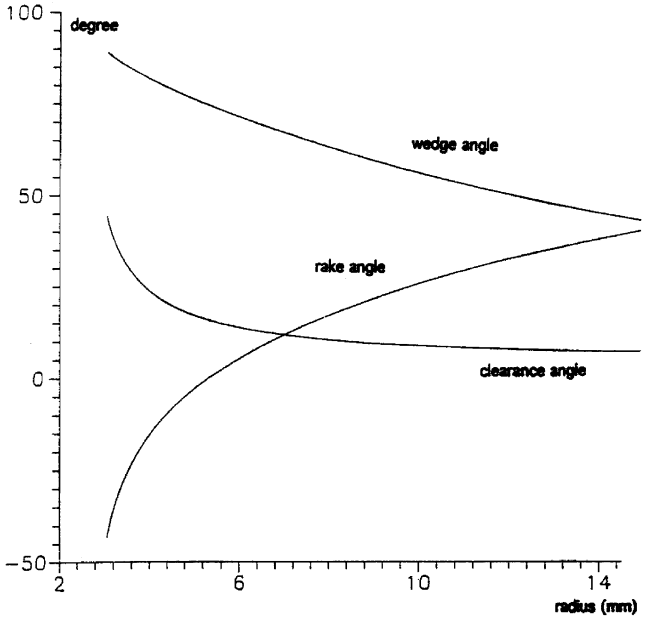

Fig. 9. The rake angle and clearance angle of points along the first cutting edge.

8. Grinding

In order to verify the validity of the developed methodology, a designed three-fluted drill possessing the parameters $\alpha = 10^\circ$, $\lambda = 38^\circ$, $R = 15$, $a_{xo} = 45.5$, $k_1 = 0.286$, $k_3 = 19.098$, $m = 0$ was ground on a universal tool-grinding machine (Fig. 10) by using the grinding tool of Eq. (14). A photograph of its transverse sections at $r_{iz} = -10$ mm is shown in Fig. 11, is used for comparison with Fig. 4.

In order to generate the ith flank surface, one can obtain the relative configuration of the tool's frame with respect to drill's frame from eqs. (1) and (18) as

$$\begin{aligned} R_{flank,i} &= {}^{\circ}\Lambda_{t'i}\,{}^{t}r = \\ &[\mathrm{Rot}(z,-\beta_i)\mathrm{Trans}(0,g,0)\mathrm{Trans}(0,0,-w) \\ &\mathrm{Rot}(y,-\Psi)\mathrm{Trans}(0,0,\lambda)][\mathrm{Rot}(z,v)\,{}^{t}q] = \\ &[\mathrm{Rot}(z,-\beta_i)\mathrm{Trans}(0,g,0)\mathrm{Trans}(0,0,-w) \\ &\mathrm{Rot}(y,-\Psi)\mathrm{Trans}(0,0,\lambda)\mathrm{Rot}(z,v)]\,{}^{t}q \end{aligned} \tag{35}$$

Eq. (35) indicates that one can produce the ith flank surface if the universal tool-grinding machine can position the workpiece at configuration $\mathrm{Rot}(z,-\beta_i)\mathrm{Trans}(0,g,0)\mathrm{Trans}(0,0,-w)\mathrm{Rot}(y,-\Psi)\mathrm{Trans}(0,0,\lambda)$ and provide the an additional rotational motion $\mathrm{Rot}(z,v)$, while the grinding tool possesses the generating curve ${}^{t}q$. In fact, the grinding tool doesn't have to revolve 360°, since the active cutting area of the ith flank is smaller than 120°. Fig. 12 gives the front end view of the major cutting edges.

9. Concluding remarks

A simple and complete multiflute drill model, which has been previously unavailable in the literature, is presented explicitly in this paper. This model contains a flute model and a general flank model having $z = f(x)$

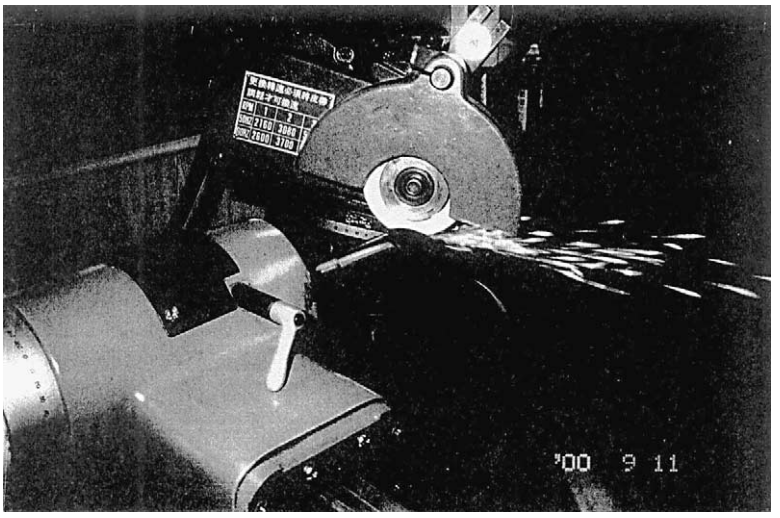

Fig. 10. Grinding a three-fluted drill on a universal tool-grinding machine.

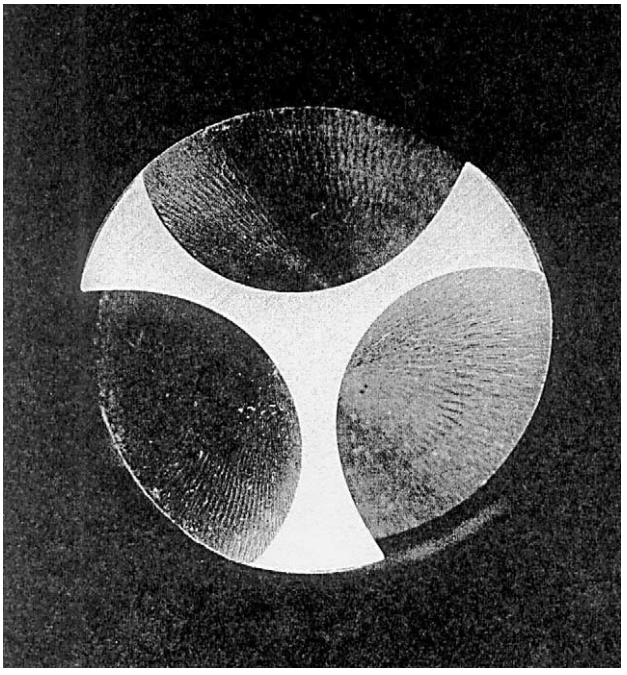

Fig. 11. The transverse section of the ground drill at $r_{iz}=-10$ mm.

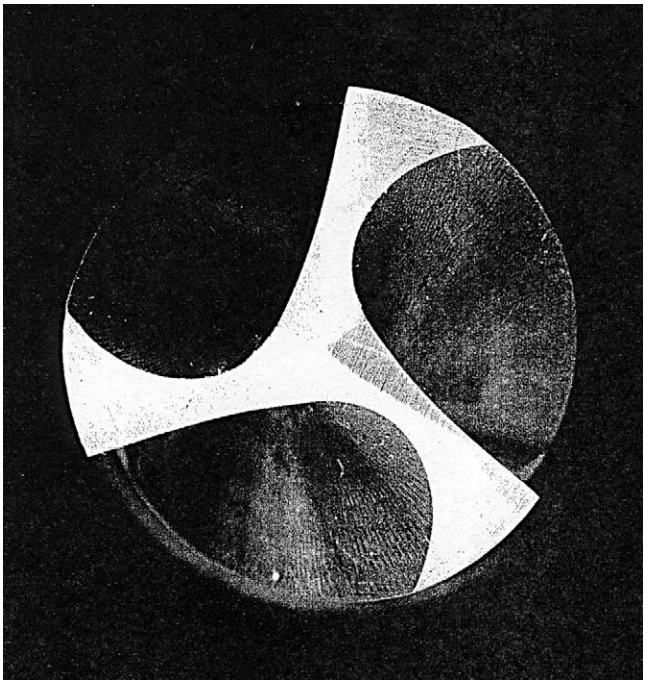

Fig. 12. The front end view of the drill's major cutting edges.

as it generating curve. Therefore, the proposed model can be reduced to conical, elliptical, hyperbolic and parabolic drill grinding models. The proposed model contains three basic features. First, rotational axial-type cutting tools and disk-type abrasive wheels are modeled by revolution geometry, thus allowing the normals and tangent vectors of flute and flank surfaces to be obtained explicitly. Consequently, rake and clearance angles of cutting and chisel edges can be investigated according recommended ISO standards. Second, the mathematical models of flute and flank surfaces are integrated, so that cutting and chisel edges and their various characteristic angles can be obtained by numerical calculation. Third, a simple way to determine the rake angles and wedge angles and clearance angles is presented by using the unit normals of the ISO-recommended reference planes, allowing the major cutting edges and chisel edges and their various cutting angles to be investigated according to ISO recommendations. To verify the validity of the method, the proposed approach was implemented in software and used to design a three fluted drill. Then the Denavit–Hartenberg notation was employed in the determination of the desired NC data for a 6-axis tool-grinding machine used in drill production. Better understanding of the multiflute drill can be achieved based on this mathematical model. In the future, a drill having

a desired rake angle distribution will be developed by searching for the optimum generating curve.

Acknowledgements

The authors are thankful to the National Science Council of Taiwan for supporting this research under grant NSC89-2212-E-006-167. Our sincere thanks also go to lecturer Yi Wu Chao of Far-East Institute of Technology for his assistance in conducting the experimental work.

Appendix

$$\mathrm{Rot}(z,\nu) = \begin{bmatrix} C\nu & -S\nu & 0 & 0 \\ S\nu & C\nu & 0 & 0 \\ 0 & 0 & 1 & 0 \\ 0 & 0 & 0 & 1 \end{bmatrix} \quad \text{(A1)}$$

$$\mathrm{Trans}(a_x,a_y,a_z) = \begin{bmatrix} 1 & 0 & 0 & a_x \\ 0 & 1 & 0 & a_y \\ 0 & 0 & 1 & a_z \\ 0 & 0 & 0 & 1 \end{bmatrix} \quad \text{(A2)}$$

$$\mathrm{Rot}(x,\lambda) = \begin{bmatrix} 1 & 0 & 0 & 0 \\ 0 & C\lambda & -S\lambda & 0 \\ 0 & S\lambda & C\lambda & 0 \\ 0 & 0 & 0 & 1 \end{bmatrix} \quad \text{(A3)}$$

$$\mathrm{Rot}(y,\alpha) = \begin{bmatrix} C\alpha & 0 & S\alpha & 0 \\ 0 & 1 & 0 & 0 \\ -S\alpha & 0 & C\alpha & 0 \\ 0 & 0 & 0 & 1 \end{bmatrix} \quad \text{(A4)}$$

$$^{i-1}\underline{\underline{A}}_i = \begin{bmatrix} C\theta_i & -S\theta_i C\alpha_i & S\theta_i S\alpha_i & a_i S\theta_i \\ S\theta_i & C\theta_i C\alpha_i & -C\theta_i S\alpha_i & a_i S\theta_i \\ 0 & S\alpha_i & C\alpha_i & b_i \\ 0 & 0 & 0 & 1 \end{bmatrix} \quad \text{(A5)}$$

References

[1] D.S. Sheth, S. Malkin, CAD/CAM for geometry and process analysis of helical groove machining, Annals of the CIRP 39 (1) (1990) 129–132.
[2] J. Agullo-Batlle, S. Cardona-Foix, C. Vinas-Sanz, On the design of milling cutters or grinding wheels for twist drill manufacture. A CAD approach, in: Proc. of the Twenty Fifth Machine Tool Design and Research Conference, 1985, pp. 315–320.
[3] S.K. Kang, K.F. Ehmann, C. Lin, A CAD approach to helical groove machining. Part I: mathematical model and model solution, Int. J. Mach. Tools Manufact. 36 (1996) 141–153.
[4] E.J.A. Armarego, J.D. Wright, An analytical study of three point grinding methods for general purpose twist drills, Annals of the CIRP 29 (1980) 5–10.
[5] D.F. Galloway, Some experiments on the influence of various factors on drilling performance, Transactions of the ASME 79 (1956) 191–231.
[6] H. Ernst, W.A. Haggerty, The spiral point drill—a new concept in drill point geometry, Transactions of the ASME July (1958) 1059–1072.
[7] M.A. Fugelso, Cylindrical flank twist drill points, ASME Journal of Engineering for Industry 105 (1983) 183–186.
[8] S.M. Wu, J.M. Shen, Mathematical model for multifacet drills, ASME Journal of Engineering for Industry 105 (1983) 177–182.
[9] T. Radhakrishnan, R.K.K. Kawlra, S.M. Wu, A mathematical model of the grinding wheel profile required for a specific twist drill flute, Int. J. Mach. Tools Manufact. 22 (4) (1982) 239–251.
[10] C. Lin, S.K. Kang, K.F. Ehmann, Helical micro-drill point design and grinding, ASME Journal of Engineering for Industry 117 (3) (1995) 277–287.
[11] S. Fujii, M.F. DeVries, S.M. Wu, An analysis of drill geometry for optimum design by computer. Part I—drill geometry analysis, ASME Journal of Engineering for Industry 92 (3) (1970) 647–656.
[12] S. Fujii, M.F. DeVries, S.M. Wu, An analysis of drill geometry for optimum design by computer. Part II—computer aided design, ASME Journal of Engineering for Industry 92 (3) (1970) 657–666.
[13] S. Fujii, M.F. DeVries, S.M. Wu, An analysis of of the chisel edge and the effect of the d-theta relationship on drill point geometry, ASME Journal of Engineering for Industry 93 (4) (1971) 1093–1105.
[14] W.D. Tsai, S.M. Wu, A mathematical model for drill point design and grinding, Int. J. Mach. Tools Manufact. 19 (1) (1979) 109–120.
[15] S.J. Lin, K.F. Eman, S.M. Wu, An analysis of the drill wandering motion, ASME Journal of Engineering for Industry 109 (4) (1987) 297–305.
[16] W.D. Tsai, S.M. Wu, Measurement and control of the drill point grinding process, ASME Journal of Engineering for Industry 101 (1979) 333–340.
[17] S. Ema, H. Fujii, E. Marui, S. Kato, New type drill with three major cutting edges, Int. J. Mach. Tools Manufact. 28 (4) (1988) 461–473.
[18] S. Ema, H. Fujii, E. Maruit, Cutting performance of drills with three cutting edges (effects of chisel edge shapes on the cutting performance), Int. J. Mach. Tools Manufact. 31 (3) (1991) 361–369.
[19] J.S. Agapiou, Design characteristics of new types of drill and evaluation of their performance drilling cast iron—I. Drill with Four major cutting edges, Int. J. Mach. Tools Manufact. 33 (3) (1993) 321–341.
[20] J.S. Agapiou, Design characteristics of new types of drill and evaluation of their performance drilling cast iron—II. Drill with three major cutting edges, Int. J. Mach. Tools Manufact. 33 (3) (1993) 343–365.
[21] Paul, 1982.
[22] Dhande, Chakrabarty, 1976.
[23] G. Boothroyd, Fundamentals of metal machining and machine tools, in: McGraw-Hill, Englewood Cliffs, NJ, 1975.